JOURNAL OF GEOPHYSICAL RESEARCH, VOL. 108, NO. A4, 1158, doi:10.1029/2002JA009286, 2003

Implications of the observed anticorrelation between solar wind speed and coronal electron temperature

George Gloeckler[1]

Department of Physics/Space Physics and Institute for Physical Science and Technology, University of Maryland, College Park, Maryland, USA

Thomas H. Zurbuchen

Department of Atmospheric, Oceanic, and Space Sciences, University of Michigan, Ann Arbor, Michigan, USA

Johannes Geiss

International Space Science Institute, Bern, Switzerland

Received 28 January 2002; revised 13 November 2002; accepted 24 January 2003; published 19 April 2003.

[1] Electron temperatures at the source of the solar wind are now obtained routinely and continuously from measurements of charge states of solar wind ions with modern solar wind composition spectrometers over a wide range of solar wind speeds. While the general anticorrelation between solar wind speed and electron temperature was previously noted, the physical processes responsible for this anticorrelation were not well understood, nor were mechanisms proposed that would produce this observed anticorrelation. We present a detailed analysis of solar wind measurements made with the Solar Wind Ion Composition Spectrometer (SWICS) on Ulysses over nearly an entire solar cycle and the full latitude range of Ulysses. We show that the electron temperature, T, derived from the O^{7+}/O^{6+} density ratios, is not only well anticorrelated with measured solar wind speed, V_{sw}, in general, but also that the dependence of V_{sw} on $1/T$ is well represented by the solar wind equation derived by *Fisk* [2003]. This equation is based on the simple model in which the plasma of both the fast and slow wind is released from magnetic loops, which are opened by reconnection with open field lines. Fitting these SWICS data to the Fisk equation, we infer the dependence on loop height of the ratio of the magnetic field strength to mass density near the base of the loops (at the altitude of reconnection) and infer the solar cycle and latitude dependence of the size of the loops and of the strength of the average open field. We suggest that the same simple mechanism can account for both the fast and slow solar wind and that the final speed of the solar wind is determined primarily by the electron temperature in magnetic loops on the Sun, from which the solar wind originates. *INDEX TERMS:* 7835 Space Plasma Physics: Magnetic reconnection; 2169 Interplanetary Physics: Sources of the solar wind; 2162 Interplanetary Physics: Solar cycle variations (7536); 2164 Interplanetary Physics: Solar wind plasma; *KEYWORDS:* solar wind, coronal electron temperature, solar north-south asymmetries, solar wind speed and temperature correlations, freezing-in temperatures, Ulysses-SWICS observations

Citation: Gloeckler, G., T. H. Zurbuchen, and J. Geiss, Implications of the observed anticorrelation between solar wind speed and coronal electron temperature, *J. Geophys. Res.*, *108*(A4), 1158, doi:10.1029/2002JA009286, 2003.

1. Introduction

[2] That the solar wind bulk speed is generally anticorrelated with the coronal electron temperature is now reasonably well established from measurements: first with the ion mass/charge spectrometer on the ISEE 3 spacecraft [*Ogilvie et al.*, 1989] and then, more definitively, with the Solar Wind Ion Composition Spectrometer (SWICS) on Ulysses [*Geiss et al.*, 1995], which sampled both the ecliptic slow wind as well as the polar coronal hole fast wind at higher latitudes. This observed anticorrelation was attributed to the fact that the fast wind is accelerated in the cool coronal holes, whereas the slow wind comes from hotter regions in the solar corona. The underlying causes for the anticorrelation between solar wind speed and coronal temperature were not known. Using an extensive set of SWICS composition data, we show that the measured speed of the solar wind is related in a simple fashion to the electron temperature (derived from measured charge states of solar wind ions such as the O^{7+}/O^{6+} density ratio)

[1]Also at Department of Atmospheric, Oceanic, and Space Sciences, University of Michigan, Ann Arbor, Michigan, USA.

0148-0227/03/2002JA009286

at the origin of that wind. More specifically, we find that the square of the solar wind speed, V_{sw}^2, follows a simple curve when plotted as a function of the inverse of the electron temperature, T. This relationship is clearly revealed during periods of large changes in V_{sw} and T seen at the edges of the large polar coronal holes during solar minimum. Significant deviations from this simple curve occur only during long-duration coronal mass ejections (CMEs).

[3] An explanation of the observed dependence of V_{sw}^2 on $1/T$ is given by *Fisk* [2003], who suggests that the solar wind originates in closed magnetic loops and that the energy to accelerate the solar wind comes from the reconnection of open field lines with closed magnetic loops near the surface of the Sun. We first test Fisk's simple solar wind formula using the SWICS data. Next, we infer the dependence of the ratio of loop magnetic field strength to mass density on loop size. Finally, we examine the solar cycle and latitude dependence of the average loop heights and the average open magnetic field strength inferred from the data. We conclude that the difference in the speed and charge states between the fast and slow solar wind is not the result of different acceleration mechanisms but rather can be attributed to differences in the temperature of electrons in solar magnetic loops.

2. Observations of the Solar Wind

[4] For this study we use measurements of solar wind parameters from the SWICS instrument on Ulysses. This SWICS-Ulysses combination provides a most powerful tool with which to study a variety of solar and heliospheric phenomena not previously possible. Ulysses is the first spacecraft to explore a wide range of heliolatitudes (0 to $\pm 80^\circ$), and SWICS continuously measures the solar wind speed and the ionization states used to derive electron temperature at the source of the solar wind every 12 min. The Ulysses orbit allows us to sample both the in-ecliptic and the high-latitude solar wind over a large fraction of the solar cycle. Of particular importance for this study are the time periods when Ulysses makes the periodic transitions through the boundary between the large polar coronal holes and the quiet Sun. During these relatively short time periods, large changes are observed in both the solar wind speed and coronal electron temperature at nearly constant latitude [*Geiss et al.*, 1995].

[5] In the SWICS instrument we combine energy/charge analysis followed by postacceleration (to $\sim$23 keV) with a time-of-flight and energy measurement to determine the mass, charge or ionization state, and energy of ions from $\sim$0.6 to $\sim$60 keV/e [see *Gloeckler et al.*, 1992]. This allows us to measure the bulk speeds and densities of the more abundant solar wind ions, including O^{6+} and O^{7+}, under all solar wind conditions in both the fast and slow solar wind [e.g., *Zurbuchen et al.*, 2002]. For this study we use 12-hour averages of the solar wind proton speed and the O^{7+}/O^{6+} density ratios as our basic data, spanning a 10-year time period from 7 December 1990 (day of year 1990 (DOY1990) = 341) to 31 December 2000 (DOY1990 = 4017). Averaging intervals of at least 12 hours was necessary in order to obtain statistically significant O^{7+}/O^{6+} density ratios at low coronal electron temperatures.

[6] From the O^{7+}/O^{6+} ratios we derive the electron temperature at the source of the solar wind using the equilibrium model of *Ko et al.* [1997]. In this model the electron temperature increases monotonically, with an increasing O^{7+}/O^{6+} ($\equiv R_O$) ratio. For example, $T = 1 \times 10^6$ K for $R_O = 0.0091$ and $T = 1.7 \times 10^6$ K for $R_O = 0.4$. The typical measurement error of T (assuming that the coronal electron temperature remains constant over 12-hour intervals) is $\sim$4.2% for $T \approx 1 \times 10^6$ K and 3.2% for $T \approx 1.7 \times 10^6$ K. The statistical uncertainty in measuring V_{sw} is $\sim$1.5%.

[7] In Figure 1 we show variations with time of $1/T$ and of V_{sw} during six solar rotations (27 August 1996 to 9 February 1997). During this short time period (compared with the 11-year solar cycle), Ulysses stayed at a nearly constant latitude $\sim(+30 \pm 5)^\circ$ and periodically crossed the boundary between the fast solar wind from the large northern polar coronal hole and the slow wind outside the coronal hole. SWICS was sampling solar wind conditions over a wide range of solar wind speeds at nearly constant latitude and time, thus minimizing latitude and solar-cycle-dependent variations.

[8] The $1/T$ curve matches the solar wind speed curve remarkably well, not just at high or low speeds but also during the fast transitions from low to high speeds and vice versa. The only time periods when the tracking is significantly disrupted are indicated by the shaded regions in Figure 1. During these two time periods the Solar Wind Observations Over the Poles of the Sun (SWOOPS) instrument on Ulysses measured extensive bidirectional electron anisotropies and identified these periods as CME events lasting $\sim$7–9 days (J. Gosling, personal communication, 2002). Bidirectional electron anisotropies of much shorter duration were also observed by SWOOPS on other days in January and February 1997 (J. Gosling, personal communication, 2002). For these smaller events the $1/T - V_{sw}$ correlation was not significantly disrupted.

[9] Except for the two long-duration CME periods, V_{sw} is observed to track $1/T$ to within $\sim$10–15% of the measured speed. This is somewhat surprising. The electron temperature computed from the O^{7+}/O^{6+} ratio represents conditions close to the Sun. Charge states of solar wind ions are not expected to change after they "freeze in" at a few solar radii. The solar wind speed, on the other hand, is expected to change in transit from the inner heliosphere to several AU due to, for example, stream-stream interactions. In fact, the rapid increases in speed on days 275 and 327, for example, contain forward and reverse shocks (or waves) of corotating interaction regions (CIRs) [*Gosling and Pizzo*, 1999; *Gloeckler*, 1999]. There were also relatively strong forward and reverse waves/shocks on the leading edges of all the other streams shown in Figure 1 (J. Gosling, personal communication, 2002). These waves/shocks were clearly not present close to the Sun.

[10] It is equally surprising, but still the case, that deviations of V_{sw} from $1/T$ are not larger at the leading edges of fast streams or in the slow solar wind than they are in the solar wind from coronal holes. One would have expected that speed changes in the quiet, least turbulent solar wind from polar coronal holes would be smaller than speed changes in the more perturbed slow solar wind [*Gloeckler*, 1999], especially in the solar wind of leading edges of fast streams. Nevertheless, our 36-hour running averaged data

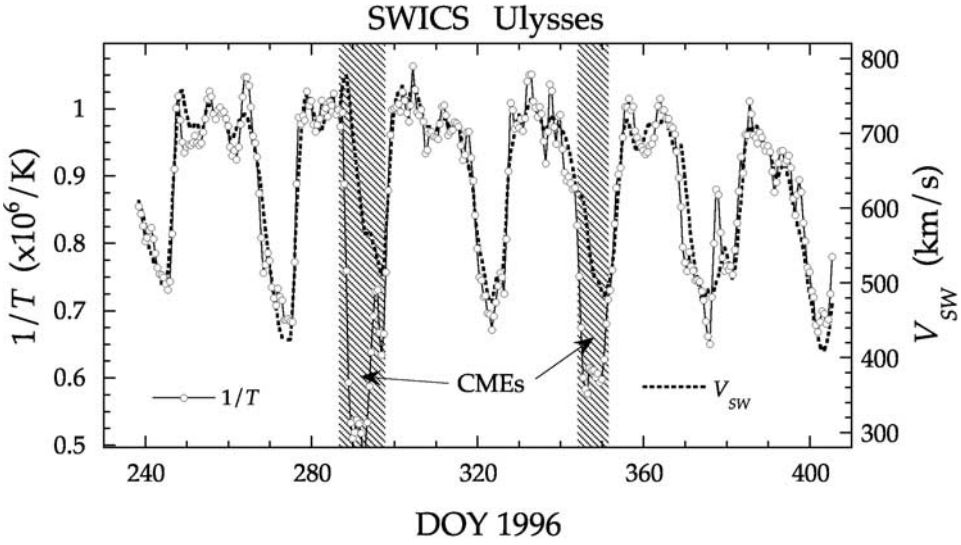

Figure 1. Time variations of the inverse of the electron temperature, $1/T$, in units of 10^6 K (open circles) and of the solar wind proton bulk speed, V_{sw}, in units of km s^{-1} (dotted curves) during a 166-day time period (27 August 1996 to 9 February 1997), observed with the Solar Wind Ion Composition Spectrometer (SWICS) on Ulysses. The data are three-point running averages of the basic 12-hour averages. The tracking of the $1/T$ and V_{sw} curves is almost perfect except during the two time periods indicated by the shaded regions. Each of these two time periods coincides with a long-duration coronal mass ejection (CME) event, identified using bidirectional electron signatures in the Ulysses Solar Wind Observations Over the Poles of the Sun (SWOOPS) data (J. Gosling, personal communication, 2002).

show that except for the solar wind in long-duration CMEs, V_{sw} tracks $1/T$ to within less than ~15%, even in presumably the most perturbed solar wind in the leading edges of fast streams.

[11] The data presented in Figure 1 show an underlying strong correlation between V_{sw} and $1/T$. Excluding the two long-duration CME periods indicated by the shaded regions of Figure 1, a least squares fit to the remaining data, assuming a linear relation of the form $V_{sw} = \langle B^* \rangle / T - V_o$, gives

$$V_{sw} = 844/T - 88, \quad (1)$$

with units of km s^{-1} for V_{sw} and 10^6 K for T. In the following sections we will test the solar wind formula derived by *Fisk* [2003], which predicts a specific relationship between V_{sw}^2 and $1/T$.

3. Fisk's Solar Wind Model

[12] The Fisk solar wind model is described in detail in the companion paper [*Fisk*, 2003]. Here we summarize the essential features of this model, which is based on a set of simple principles.

[13] 1. Magnetic loops are observed to occur everywhere on the Sun; they are believed to result from small bipolar magnetic fluxes, which emerge through the solar surface and coalesce with each other by reconnection to form bigger loops [e.g., *Handy and Schrijver*, 2001]. In coronal holes the loops are relatively small (heights <15,000 km) and cool (<800,000 K); outside of coronal holes the loops on the quiet Sun are larger (heights 40,000–400,000 km) and hotter (~1.5×10^6 K) [*Feldman et al.*, 1999].

[14] 2. Open field lines (magnetic field lines which open into the heliosphere) are present among the loops, with strong concentrations in coronal holes, but are also distributed throughout the quiet Sun in lesser strength.

[15] 3. An open field line can reconnect with the end of a loop with opposite magnetic polarity, presumably near the loop base, with three consequences: (1) The loop is effectively eliminated (a small secondary loop is created that appears to subduct back into the photosphere). (2) The open field line is displaced to lie over the location of the side of the original loop with the same polarity. (3) Mass is released from the loop onto the open field line.

[16] 4. The displacement of the open field line will disturb the overlying corona. Magnetic pressure variations will be introduced. When the coronal magnetic field relaxes back into equilibrium, work is done, and energy is assumed to be deposited into the corona in the form of heat. The amount of energy that is deposited can be readily calculated [*Fisk*, 2003].

[17] 5. The mass that is released through the reconnection process depends on the mass available in the loop. If the loops are isothermal, the available mass depends mainly on the scale height, which in turn depends on the isothermal temperature. The relationship between available mass and temperature is linear, except for loop heights that are comparable to the scale height, in which case a small correction factor is required.

[18] 6. The energy that is supplied can be represented as a Poynting vector into the corona. Loops emerge through the solar surface and thus represent an upward Poynting vector, for which there is no comparable downward Poynting vector since the loops are in large part eliminated by the

reconnection with open field lines. The mass supplied through the reconnection process will determine the mass flux of the solar wind.

[19] 7. A simple energy balance equation can be used to specify the final solar wind speed squared, u_f^2, in terms of the Poynting vector and mass flux. It yields a unique formula [*Fisk*, 2003, equation (11)] that predicts that the speed squared varies essentially linearly as the inverse of the loop temperature T:

$$Y = AX\beta(h, T) - Y_o, \tag{2}$$

where $Y = (u_f^2)/2$, $X = GMm/(2r_skT)$, and $Y_o = GM/r_s$ and is a constant. G is the gravitational constant, M is the mass of the Sun, r_s is the radius of the Sun, m is the proton mass, k is the Boltzmann constant, h is the height of the loop above the point of reconnection, and $\beta(h,T)$ is the correction factor described below. Substituting numerical values for M, m, r_s and k results in $Y_o = 1.908 \times 10^{15}$ (cm s^{-1})^2 and $X = 11.55/T$, with T in units of 10^6 K. The variable X is dimensionless.

[20] The quantity $A = (B/\rho)_{\rm loop}(\int \mathbf{B}_{\rm open} \cdot d\mathbf{l})(4\pi r_s)^{-1}$, where $(B/\rho)_{\rm loop}$ is the ratio of the magnetic field strength to the mass density of the loop at the base, where the reconnection with the open field line presumably occurs [*Fisk*, 2003], and $\int \mathbf{B}_{\rm open} \cdot d\mathbf{l}$ is an integral along the open magnetic field from the surface of the Sun to large distances, where $B_{\rm open}$ becomes negligible ($d\mathbf{l}$ is the line element along the path of integration). *Fisk* [2003] points out that if the open magnetic field in the corona can be described as a potential field, this integral will be approximately constant for all open field lines regardless of whether they undergo a radial or a superradial expansion. If there is radial expansion, the integral $\int \mathbf{B}_{\rm open} \cdot d\mathbf{l} \approx B^*_{\rm open}(r_s^*/r_s)^2 r_s$ [see *Fisk*, 2003], where $B^*_{\rm open}$ is the open magnetic field strength at an altitude r_s^* of several solar radii where that field becomes radial. The quantity $B^*_{\rm open}$ is related to the radial component of the magnetic field magnitude, B_r, at 1 AU as $B^*_{\rm open} = B_r(r_1/r_s^*)^2$, where r_1 = 1 AU = 215.5 r_s. With the measured $B_r \approx 3 \times 10^{-5}$ G being reasonably constant during the solar cycle and with latitude [*Smith and Balogh*, 1995], $B^*_{\rm open} \approx 1.4\ (r_s/r_s^*)^2$ G and is also approximately constant. The quantity A in equation (2) then reduces to

$$A \approx (1.4/4\pi)(B/\rho)_{\rm loop}. \tag{3}$$

[21] The correction factor, $\beta(h, T)$, is $[1 - \exp(-1.75hX/r_s)]^{-1}$ [*Fisk*, 2003]. For loops on the quiet Sun, *Feldman et al.* [1999] find that the height of loops increases with increasing temperature of the material in the loops: Hotter loops overlie cooler ones. Therefore $\beta(h, T)$ should primarily be a function of temperature, although not a strong one since, as discussed above, loop height increases with T, while X is inversely proportional to T. In the case of low loops on the Sun, protons and electrons should be collisional and thus have equal temperatures. As the ions are released from the loops by reconnection, collisions will no longer be important, and the ions and electrons can then achieve different temperatures in the corona.

[22] Thus, provided that the quantity $(B/\rho)_{\rm loop}$ is relatively constant on the Sun and $\beta(h, T)$ depends only weakly on T, Fisk's theory for the acceleration of the solar wind predicts that the final speed of the solar wind depends on only one parameter, the temperature of the material in the originating loops, and that the final speed squared varies essentially linearly as $1/T$. The quantity $(B/\rho)_{\rm loop}$ would, in fact, be relatively constant if loops expand such that the density and magnetic field strength stay proportional to one another [see *Rosner*, 1990, and references therein].

[23] The dependence on loop temperature in equation (2) arises simply because the available mass, and thus the mass flux, is proportional to the scale height, which in turn is proportional to temperature. The final speed squared of the solar wind varies inversely with the mass flux. Equation (2) should hold in all forms of the solar wind: fast solar wind from coronal holes, where the loops involved are smaller and cooler, and slow solar wind from elsewhere on the quiet Sun, where the loops are larger and hotter.

[24] Equation (2) requires knowledge of the actual loop temperature. We observe the solar wind ionic charge states and from that determine the electron temperature at the point in the corona where the charge states freeze in. It is not unreasonable that these two temperatures will be nearly identical. First, coronal loops that we presume are opened up to provide the solar wind are observed to have temperatures comparable to those inferred from solar wind charge states. A typical, relatively large coronal loop on the quiet Sun, which should provide the slow solar wind, is observed to have temperatures $\sim 1.5 \times 10^6$ K [e.g., *Feldman et al.*, 1999], whereas the coronal electron temperature inferred from charge states in the slow solar wind is $\sim 1.7 \times 10^6$ K [*von Steiger et al.*, 2000]. Similarly, the smaller loops that provide the fast solar wind have temperatures of $\sim$800,000 K, whereas the temperature inferred from charge states is $\sim 1.0 \times 10^6$ K. These apparent systematic differences could result from the reconnection process itself, when the open field line reconnects with the loop. A small amount of heat could be imparted to the loop. The actual mass release process itself, in which there is a sudden drop in density, could facilitate the freeze-in of ionic charge states at the point of release. Conversely, the free flow of electrons along the open field lines could preserve the electron temperature near the loop value, and the freeze-in would then occur at the more traditional distances of a few solar radii [e.g., *Bürgi and Geiss*, 1986; *Geiss et al.*, 1995]. In the detailed numerical model of N. A. Schwadron (A model for acceleration of the solar wind due to the emergence of magnetic flux, submitted to *Journal of Geophysical Research*, 2002) the calculated solar wind charge states are found to be representative of the electron temperatures in the loops. Protons, in contrast, need to be heated in the corona by the dissipation of the energy imparted by the displaced open field lines in order to form the solar wind. In Fisk's model, as in conventional models, the steady state solar wind has a critical point solution, as first proposed by *Parker* [1958].

[25] All that is required to test equation (2) using SWICS observations is a one-to-one relationship between the coronal electron temperature inferred from charge state measurements and the actual temperature of electrons in the loops. For example, if these two temperatures differ by a constant amount, there is no change in the use of equation (2) to relate observed solar wind speed to freezing-in temperature from observed charge states other than a small adjustment to

the inferred dependence of loop heights on electron temperature in that loop.

4. Results

[26] The solar wind formula derived by *Fisk* [2003] (equation (2) above) basically predicts a linear dependence of u_f^2 on $1/T$. As discussed above, the β factor, which also depends on $1/T$ and loop height h, is only a small correction factor to the basic linear form. We know of no other solar wind model or theory that specifically predicts a relationship between T and u_f.

[27] Data shown in Figure 1 imply that the measured solar wind speed, V_{sw}, averaged over time periods of 36 hours (three-point running average of 12-hour data) may be used to estimate the final speed, u_f, in Fisk's formula to within $\sim$15%. As is evident from Figure 1, this appears to be the case even in the leading edges of high-speed streams that contain forward and reverse shocks/waves. We point out that the common practice of ballistic mapping of speed back to the Sun is also based on the assumption that the solar wind speed changes little in transit.

[28] In Figure 2 we show a scatterplot of $Y = (V_{sw}^2)/2$ versus $X = GMm/(2r_skT)$ using the data of Figure 1 but excluding the two CME periods indicated by the shaded regions. The 277 points in the scatterplot, as well as the 10 bin-averaged values of these points (solid circles), show a linear relationship between $(V_{sw}^2)/2$ and $1/T$, as predicted by the solar wind formula. Most of the scatter of the points is likely due to changes of the solar wind speed in transit from the several tens of solar radii to several AU. A linear least squares fit to the 10 bin-averaged points gives

$$(V_{sw}^2)/2 = 4.42 \times 10^{14} X - 2.31 \times 10^{15}. \quad (4)$$

The reduced χ^2 of the fit is 0.85. This fit is shown in Figure 2 by the line labeled $Y = A * X - Y_1$. We note that the value of Y_1, determined by the fit to be 2.31×10^{15}, is close to $Y_o = GM/r_s = 1.908 \times 10^{15}$ (cm s^{-1})^2 in the Fisk formula. An alternative representation of equation (4) is

$$V_{sw} = 1008(1/T - 0.454)^{1/2}, \quad (5)$$

with V_{sw} in units of km s^{-1} and T in units of 10^6 K.

[29] The linear dependence of $Y = (V_{sw}^2)/2$ on $1/T$ (equation (4)) is seen to be an excellent fit to the data, implying that the product $A\beta(h, T)$ in Fisk's formula (equation (2)) is nearly constant. Another way to show the linear relation of V_{sw}^2 and $1/T$ is to plot $A^* \equiv 2.25 \times 10^{-15}\ (Y + Y_1)/X$ using the data of Figure 1, where $Y = (V_{sw}^2)/2$ and $Y_1 = 2.31 \times 10^{15}$. The quantity A^* is related to $V_{sw}^2)T$ and is approximately equal to $A\beta(h, T)$ in Fisk's formula. The result is shown in Figure 3a. Excluding the two CME time periods shown as dotted curves, A^* is remarkably constant both in the low- and high-speed wind. The standard deviation, σ, of A^* is 4.63%, a value that is not much larger than the measurement uncertainty of T. Figure 3b is a plot of $B^* \equiv 1.18 \times 10^{-3}\ (V_{sw} + 88)\ T$, representing the linear relationship (equation (1)) between V_{sw} and $1/T$ suggested by Figure 1. The curves in Figures 3a and 3b are hardly distinguishable from one another, implying that the data are

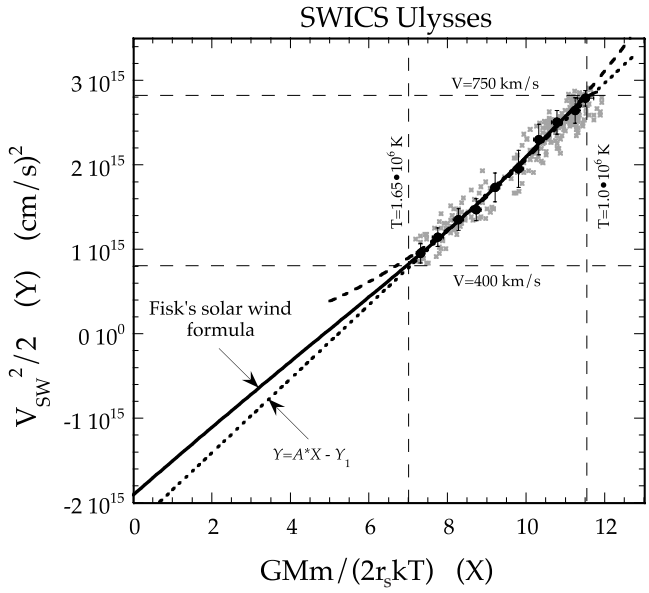

Figure 2. Scatterplot (shaded crosses) of $Y = (V_{sw}^2)/2$ versus $X = GMm/(2r_skT)$, using the data of Figure 1 except for the two CME periods. The 10 points indicated by solid circles are averages, and their error bars are standard deviations of (X_i, Y_i) pairs binned in 10 equal X intervals. The dotted curve is a linear least squares fit to the data, the dashed curve is a plot of equation (1), and the solid curve is a fit using the Fisk formula (equation (2)), as described in the text.

as well represented by a linear relation between V_{sw} and $1/T$, as between V_{sw}^2 and $1/T$. The standard deviation of B^* (non-CME data plotted as open circles) is 4.73%. A plot of equation (1) showing a linear relation between V_{sw} and $1/T$ is shown as the dashed curve in Figure 2. In the range of measured solar wind speeds and freezing-in temperatures, both equations (1) and (4) are equally good fits to the data.

[30] Outside the two CME periods, A^* and B^* are remarkably constant despite the fact that both V_{sw} and $1/T$ show large variations with a $\sim$26-day periodicity. However, during the two CME times shown by dotted curves, A^* and B^* both increase from 1.5 to 2 times their ambient values. This increase in A^* and B^* during the CME periods is so clear that this method may give us a new way to identify long-duration CMEs. We are not aware of previous discussions of this technique, which can be easily and automatically implemented to identify systematic deviations from the ambient relationship between V_{sw} and $1/T$.

[31] Figure 3c is a plot of $C^* \equiv 2.48 \times 10^{-15}\ (Y + Y_o)/X$. This is a linear fit to the data of Figure 2 except that the intercept is now fixed at $Y_o = 2.48 \times 10^{-15}$ (cm s^{-1})^2. The curve shown is again indistinguishable from those in Figures 3a and 3b. The standard deviation of C^* (non-CME data plotted as open circles) is 4.84%. We conclude that in the limited range of V_{sw} and $1/T$ it is not possible to determine which of the three linear relations fits the data best.

[32] Pursuing further the implications of Fisk's formula, we now examine more closely the dependence of the correction term $\beta(h, T)$ in equation (2) on T. Guided by observations of electron temperatures in loops [*Feldman et al.*, 1999], we assume a simple linear relationship between

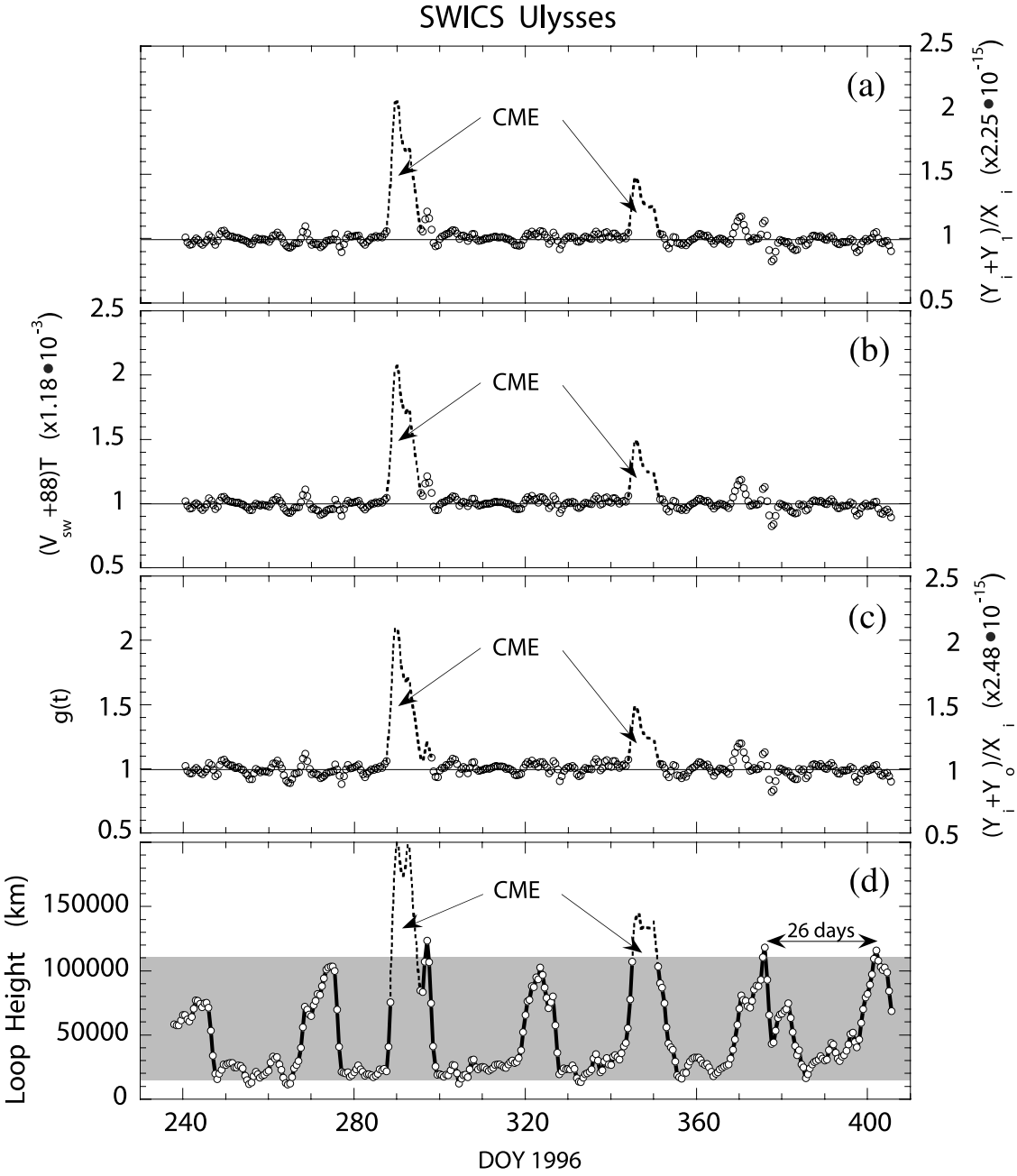

Figure 3. Plots of normalized slopes of (a) equation (4), (b) equation (1), and (c) equation (2), with $\beta = 1$, each relating either V_{sw}^2 or V_{sw} linearly with $1/T$. (d) Loop height as a function of time. The time periods for all curves are the same as those for Figure 1. Dotted curves are from the two CME periods shown as shaded regions in Figure 1. The curves in Figures 3a–3c are nearly identical, with values clustering around 1 during the non-CME periods, indicating that each of the three linear relations is a good fit to the data. During the CME periods the slopes of each of the three linear expressions increase by factors of 1.5–2. Unlike the curves in Figures 3a–3c, the inferred loop heights show a clear 26-day periodicity. The maximum loop heights of ~110,000 km are exceeded only during the two CME periods. See text for further explanation.

h, the height of the loops in units of cm, and T, the electron temperature in loops in units of 10^6 K obtained from charge state measurements of the solar wind, of the form

$$h(T) = 1.5 \times 10^9 + 1.5 \times 10^{10}(T - 1). \quad (6)$$

This fixes the height of coronal hole loops with low electron temperatures of $\sim 1 \times 10^6$ K at 15,000 km and of average loops in the quiet Sun having a typical temperature of $\sim 1.7 \times 10^6$ K at 120,000 km. These values are consistent with observations of *Feldman et al.* [1999] if the electron temperature deduced from solar wind O^{7+}/O^{6+} density ratio is systematically larger by ~200,000 K than the electron temperature found in loops from spectroscopic measurements. We assume that this systematic temperature differ-

ence exists for all loop sizes. As discussed earlier, these apparent systematic differences in temperature could result, for example, from heating of the plasma by the reconnection process itself, when the open field line reconnects with the loop. Alternatively, one could imagine that the free flow of electrons along the open field lines could preserve the electron temperature near the loop value, leading to freeze-in at the more traditional distances of several solar radii.

[33] With the linear dependence of h on T expressed by equation (6), both $h(T)$ and $\beta(T)$ become functions of only the electron temperature, T, and can be calculated using SWICS measurements of freezing-in temperatures. In Figure 3d we show the variations of calculated loop heights for the time period of Figure 1. The loop heights were computed from the temperature T using equation (6) and clearly show the ~26-day solar rotation periodicity as the edge of the north polar coronal hole rotates repeatedly past Ulysses. The minimum heights of ~15,000 km correspond to time periods when Ulysses was inside the edge of the coronal hole. The maximum loop heights of ~110,000 km (excluding the two CME periods) were reached in the quiet solar wind just outside the coronal hole. The sharp boundary of the coronal hole occurs at the often sudden decrease in loop heights from ~110,000 to ~15,000 km. During these times, CIR-associated waves/shocks occur as previously noted. In several cases (for example, DOY1996 276 and 327) the full drop takes only ~1 day. We note, however, that during times of leading edges of fast steams, corresponding to the ~26-day recurring decreases in h, no unusual features are visible in Figures 3a–3c. The calculated loop heights in the two long-duration CME periods are considerably larger, ~150,000–200,000 km.

[34] The observed linear dependence of $(V_{sw}^2)/2$ on $1/T$ requires $A\beta(h, T)$ in Fisk's formula (equation (2)) to be roughly constant. We assumed a linear relationship (equation (6)) between the loop height, h, and T consistent with observations of *Feldman et al.* [1999]. Thus, if T is a function of h, we are able to reduce $\beta(h, T)$ to $\beta(h)$ and to find the dependence of the correction term in Fisk's formula on loop height, h. From equation (3), $A = (1.4/4\pi)(B/\rho)_{loop}$ if one takes the average open field magnitude on the Sun to be constant. We assume that $(B/\rho)_{loop}$ depends on time, t, and loop height, h, such that $(B/\rho)_{loop}(t, h) = g(t)\,[(B/\rho)_{loop}(h)]$. We will see later that the dimensionless function $g(t)$ is close to unity except during CMEs. Substituting $(B/\rho)_{loop}(t, h)$ and A from equation (3) into equation (2) and solving for $(B/\rho)_{loop}(h)$ gives

$$(B/\rho)_{loop}(h) = (4\pi/1.4)[(Y + Y_o)/X]/[\beta(h)g(t)]. \quad (7)$$

[35] In Figure 4 we show a plot of $(B/\rho)_{loop}(h)$ (multiplied by 5×10^{-16}) as a function of h, using the Y and X values of Figure 1 (open circles) except for the CME periods and the binned data of Figure 2 (solid circles), which also exclude the CMEs. These are, of course, the inferred values of $(B/\rho)_{loop}$, using Fisk's formula and the observed linear dependence of $(V_{sw}^2)/2$ on $1/T$. The ratio $(B/\rho)_{loop}$ increases systematically with increasing loop height, having its smallest value in the small loops of coronal holes. If we take the density ρ_{loop} to be constant, then Figure 4 also gives the inferred dependence of the field strength in the loops, B_{loop}, on loop height; that is, a larger field strength in larger loops. One could speculate that loops grow as a result of the coalescence of smaller loops [*Handy and Schrijver*, 2001], and thus we should expect that larger loops exhibit larger field strength. On the other hand, it may actually be that the density varies and that the field strength in the loops remains more or less constant. The above speculations not withstanding, when two loops coalesce, the magnetic flux should remain the same. The field strength varies, of course, with cross-sectional area. However, it is not known at this time how this varies with loop size.

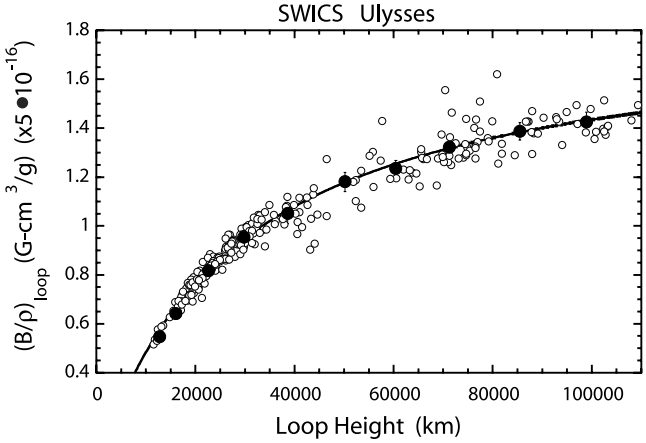

Figure 4. Inferred dependence of the magnetic field strength to mass density ratio, $(B/\rho)_{loop}(h)$, near the base of the loops where reconnection takes place, on loop height, h, obtained from fits of the solar wind formula of *Fisk* [2003] to the SWICS-Ulysses data. Error bars are computed from standard deviations of the bin-averaged Y values of Figure 2. The curve is a fit of the form $(B/\rho)_{loop}(h) = \zeta/[1 + (\mu/h)]$ to the three-point running averages (open circles) of the non-CME data of Figure 1. See text for details.

[36] If we take $B_{loop} = 25$ G in ~100,000 km loops [e.g., *Handy and Schrijver*, 2001], which corresponds to a temperature of $\sim 1.6 \times 10^6$ K using equation (6), then the mass density near the base of the loops at the location of reconnection is calculated to be 0.85×10^{-14} g cm^{-3}. The corresponding electron density at the base of these large loops would then be $n_{loop} \approx 4 \times 10^9$ cm^{-3}. These are not unreasonable values.

[37] A least squares fit to the data (Figure 4, open circles) of the form $(B/\rho)_{loop} = \zeta/(1 + [\mu/h])$ produces the result

$$(B/\rho)_{loop}(h) = 3.68 \times 10^{15}/\left[1 + \left(2.81 \times 10^9/h\right)\right], \quad (8)$$

with $(B/\rho)_{loop}$ in units of G cm^3 g^{-1} and h in units of cm. The reduced χ^2 of the fit is 0.85. The fitted curve passes through all 10 points of the binned data within their errors. The solid curve in Figure 2 is computed using Fisk's solar wind formula and equations (6) and (8) for the dependence of h on T and $(B/\rho)_{loop}$ on h, respectively. It is clearly an excellent fit to the data.

[38] The observed linear dependence of V_{sw}^2 on $1/T$ for non-CME periods is satisfied if $(B/\rho)_{loop}(h)\ \beta(h)$ is taken to be a constant. In fact, the dependence of $(B/\rho)_{loop}(h)$ on h given in equation (8) and shown in Figure 4 follows from this and the assumption that during short time periods, B^*_{open} is approximately constant, as is $g(t)$ when CME periods are excluded.

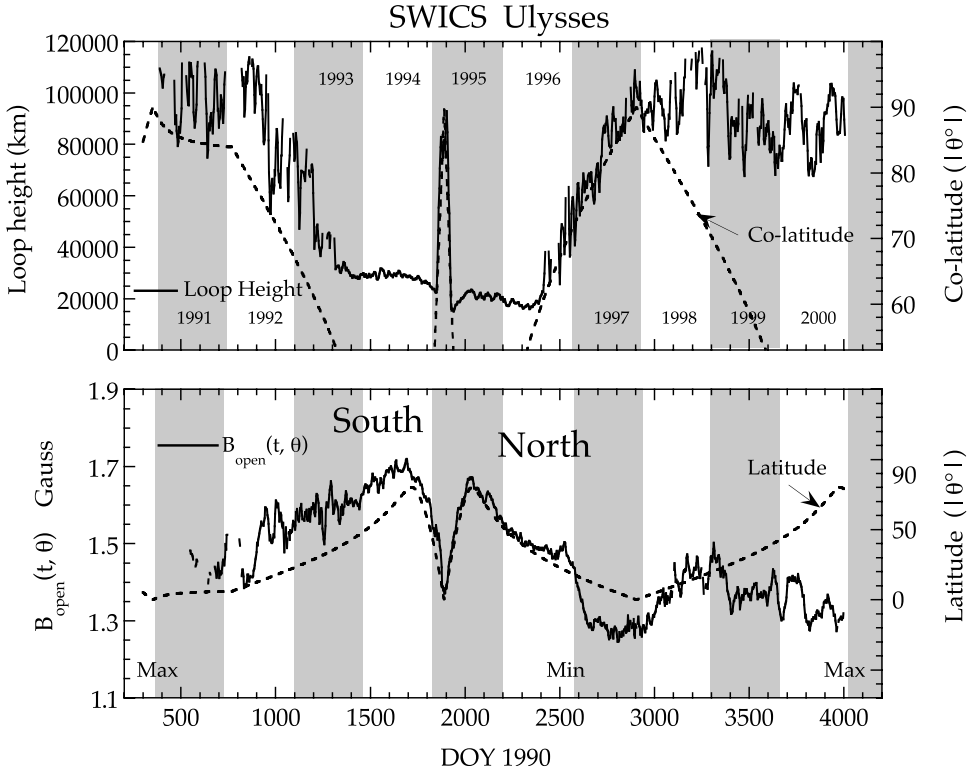

Figure 5. (top) Computed loop height, solid curve; absolute value of the colatitude of Ulysses, dashed curve. (bottom) Open magnetic field strength near the Sun where that field becomes radial, solid curve; absolute value of the latitude, dashed curve. All curves are versus day of year 1990 (odd years are indicated by shaded regions) for the ~10-year time period from 7 December 1991 to 31 December 2000. The SWICS data used here are 11-point running averages of 3-day averaged proton speeds and O^{7+}/O^{6+} density ratios used to compute electron temperature. Time periods of long-duration CME events were excluded as described in the text. The loop heights (top) show a clear colatitude dependence outside coronal holes. Inside both polar coronal holes, loop heights reach their minimum values, are nearly constant, and have few fluctuations. The most remarkable feature is the north-south asymmetry in both the loop heights and in the open magnetic field strength both inside and outside the large polar coronal holes. See text for details.

If we now assume that the systematic dependence of $(B/\rho)_{loop}(h)$ on h given by the fit (equation (8)) to the data of Figure 4 holds true for all times, including CME periods, then it follows from equation (7) that $g(t) \propto (Y + Y_o)/X$ since $(B/\rho)_{loop}(h)\ \beta(h)$ is approximately constant. The plot of $2.48 \times 10^{-15}\ (Y + Y_o)/X$ shown in Figure 3c is therefore also a plot of the temporal variations of $(B/\rho)_{loop}$. Excluding the two CME periods, $g(t)$ is indeed very close to 1 as we had earlier assumed in both the low- and high-speed wind. However, during the two CME time periods, $g(t)$ increases by about a factor of 2. We infer that the CME solar wind originates in larger than normal loops that have larger than normal (as computed from equation (8)) magnetic field strength to density ratios.

5. Discussion

[39] The 166-day-long SWICS data set used in section 4 to test Fisk's solar wind formula (equation (2)) was chosen to be relatively short in order to minimize possible latitudinal and solar cycle variations while at the same time displaying a wide range (around a factor of 2) of solar wind speeds, V_{sw}, and electron freezing-in temperatures, T. For most of our analysis we used three-point running averages of the 12-hour basic data to reduce measurement uncertainties and random variations in T and changes in V_{sw} due to effects such as stream-stream interactions that undoubtedly occurred in transit.

[40] We now apply the same procedure used in the analysis of data shown in Figures 3c and 3d to the 10-year-long SWICS-Ulysses data set. Using our basic 12-hour data, we first compute $g(t) \equiv 2.48 \times 10^{-15}\ (Y + Y_o)/X$ for the entire time period. We then eliminate time periods during which there was an increase of $g(t)$ lasting >3 days from the highly smoothed curve constructed from $g(t)$, which represents the ambient V_{sw} versus T relation. This was done in order to exclude long-duration CME periods as much as possible. In order to further reduce statistical uncertainties and minimize effects of short-term variations as well as stream-stream interactions, and thus to reveal the most persistent long-term features, we formed 3-day averages and applied smoothing techniques (11-point running averages) to the data.

5.1. Systematic Variations of Loop Heights

[41] Figure 5 (top) displays the loop height computed directly from T using equation (6) and the colatitude

(dashed curve) of Ulysses for the entire ~10-year time period. At low latitudes (high colatitudes), with Ulysses on its way to Jupiter, these loop heights range from ~85,000 to 115,000 km. There is then a latitude/colatitude-dependent decrease in loop heights up to the edges of the polar coronal holes. Once inside the coronal holes, the loop heights stay remarkably constant and vary far less than they do outside the coronal holes. In the southern coronal hole the average loop heights are higher (~27,000 km) than they are in the northern coronal hole (~20,000 km). The average loop height is also higher in the Southern Hemisphere compared with the Northern Hemisphere outside the coronal holes in the quiet Sun. We note here that this north-south asymmetry that we infer for loop heights, both in the polar coronal hole and the quiet Sun loops, comes directly from the asymmetry in the measured freezing-in temperature T through equation (6). The north-south asymmetry in T was first reported by *von Steiger et al.* [2000], who found a difference of 60,000 K between the north and south polar coronal holes. By comparing dT/dt in the two coronal holes, they concluded that the north-south asymmetry was real and not due to time variations. Higher O^{7+}/O^{6+} ratios in the north polar coronal hole are also reported by *Zhang et al.* [2002], who argue that this asymmetry is real and is not owing entirely to solar cycle variations. Here we suggest that the north-south asymmetry in T noted previously is related to differences in the average loop heights of the two polar coronal holes. It may be possible to confirm this suggestion by direct measurements of loop heights on the Sun during the time period of our observations.

[42] During the fast latitude scan (DOY1990 ~1900) the loop heights again track the colatitude remarkably well, reaching ~80,000–90,000 km at ~0° latitude (~90° colatitude). The loop height curve very clearly defines the boundaries of the coronal holes, especially during the fast latitude scan. Near these boundaries the smallest loop heights (~15,000 km at the edges of the north-polar coronal hole) are inferred. Approaching solar maximum (after DOY1990 ~3100), the latitude/colatitude dependence disappears, and no evidence of a polar coronal hole is seen.

5.2. Systematic Variations of the Open Magnetic Field Strength

[43] Figure 5 (bottom) plots the open magnetic field strength $B_{\rm open}(t, \theta) \equiv B^*_{\rm open}\ (t, \theta)\ (r_s^*/r_s)^2$, where $B^*_{\rm open}\ (t, \theta)$ is the magnetic field strength at r_s* (several solar radii) and where the field becomes radial, along with the absolute latitude of Ulysses. $B_{\rm open}(t, \theta)$ is computed using

$$B_{\rm open}(t,\theta) = 4\pi\Big[(Y + Y_o)/X\Big] \Big/ \Big[(B/\rho)_{\rm loop}(h)\beta(T)\Big] \qquad (9)$$

and equations (6) and (8) for $h(T)$ and $(B/\rho)_{\rm loop}(h)$, respectively. We stated before that the average open field strength, $B^*_{\rm open}\ (t, \theta)$, is observed to be approximately (but not strictly) constant, with an average value at r_s^* (where the field becomes radial) of 1.4 $(r_s/r_s^*)^2$ G [*Smith and Balogh*, 1995]. We have also shown that applying Fisk's formula to solar wind observations taken during a short time period and narrow latitude range allows us to determine the systematic dependence of $(B/\rho)_{\rm loop}(h)$ on loop heights h given by equation (8) and, through equation (6), on temperature T. Aside from large increases during long-duration CME events, which we have excluded from the data, $(B/\rho)_{\rm loop}$ is assumed to have no additional variations with time or latitude. Thus any long-term variations found in the quantity $[(Y+Y_o)/X]/\beta(T) = A = 1/4\pi\ (B^*_{\rm open})\ (B/\rho)_{\rm loop}$ of equations (2) and (3) we attribute to variations in $B^*_{\rm open}$.

[44] As shown in Figure 5 (bottom), during solar minimum the average open magnetic field strength at the Sun, $B_{\rm open}(t, \theta)$, computed from SWICS data using Fisk's formula, exhibits a most remarkable dependence on latitude both inside the polar coronal holes as well as outside the holes in the quiet Sun; this is especially so in the southern heliosphere, through the fast latitude scan and to midnorthern latitudes. It should be remembered that $B_{\rm open}(t, \theta)$ is an approximation to the integral $(\int \mathbf{B}_{\rm open}\cdot d\mathbf{l})/r_s$ in Fisk's formula. In the case that the open magnetic field can be approximated as a potential field and that the magnetic field comes into pressure equilibrium at several solar radii, $B_{\rm open}(t, \theta)$ is approximately the average open magnetic field near the Sun. As would be expected, then, the boundaries of the coronal holes are invisible in Figure 5 (bottom) because superradial expansion of the polar coronal hole field has already occurred. Nonetheless, there is a clear latitudinal variation, suggesting a systematic variation in the average open flux, $B_{\rm open}(t, \theta)$ or $B^*_{\rm open}(t, \theta)$, with latitude, which is worthy of further consideration. The highest values of $B_{\rm open}(t, \theta) \equiv B^*_{\rm open}(t, \theta)\ (r_s^*/r_s)^2$ (~1.65–1.7 G) are reached near the highest latitudes inside the two coronal holes. These values are ~30% higher than the lowest values (1.25 G) reached at solar minimum in 1997 after a surprisingly abrupt decrease starting at DOY1990 ~2550. The reason for this sharp drop is not known at present. After that minimum the correlation of $B_{\rm open}(t, \theta)$ with latitude disappears, and the average open field stays somewhat below ~1.5 G to the highest latitudes. It should be stated that despite these remarkable systematic variations in $B_{\rm open}(t, \theta)$, they are still relatively small. To within ~30% the inferred average open magnetic field strength is basically the same at all latitudes throughout the solar cycle.

5.3. North-South Asymmetry

[45] Perhaps the most interesting aspect of the behavior of $B_{\rm open}(t, \theta)$ is the north-south asymmetry. The inferred average open field strength in the southern latitudes of the Sun appears to be ~3–4% stronger than it is in the northern latitudes. A similar north-south asymmetry was reported by *Smith et al.* [2000] in the radial magnetic field and in cosmic rays [*Simpson et al.*, 1996]. These observations of north-south asymmetries in the radial (open) magnetic field at 1 AU and beyond are very likely related to the asymmetry that we infer for the open field at several solar radii, applying Fisk's formula to SWICS measurements of solar wind speed and electron temperature.

[46] With the disappearance of the polar coronal holes near solar maximum, $B_{\rm open}(t, \theta)$ remained weak to the highest latitudes up to the end of 2000, obscuring any repetition of the north-south asymmetry. It will be interesting to follow the variations in $B_{\rm open}(t, \theta)$ as the polar coronal holes appear again with approaching solar minimum (around 2006) to see if the pattern will be repeated, if the asymmetry will remain, and whether or not the north-south asymmetry will be reversed.

[47] We cannot exclude the possibility that some of the systematic variations we see in both the loop heights and $B_{open}(t, \theta)$ are due to solar cycle effects. However, the fact that during the fast latitude scan of Ulysses (DOY1990 ~1790–1970), asymmetries are evident in both the loop heights and $B_{open}(t, \theta)$ leads us to believe that the north-south asymmetries are real.

5.4. Comparison With Other Measurements

[48] It would be interesting to see if other measurements of solar parameters, such as the field strength, B_{loop}, and electron density, n_{loop}, in the loops, the dependence of B_{loop} on loop height, and open magnetic field strength, will support our results inferred from our solar wind observations using Fisk's formula. Magnetograph observations are, unfortunately, not too useful for measuring the field strength in the loops. They would have to be of much higher spatial resolution than currently available, and even then one would not be certain that the observed loop or loops are the ones that are reconnecting with the open field lines to form the solar wind being observed. For the open flux the problem is similar. While magnetograph measurements are generally accurate for measuring open flux in low-latitude coronal holes, where the perspective is adequate, they lack the spatial resolution to measure open flux in the presence of strong magnetic loops; that is, in regions from which the slower wind originates. Nevertheless, we hope that in the future it may be possible to establish the validity of the relationship between $(B/\rho)_{loop}(h)$ and loop heights (equation (8)) using remote-sensing observations. Determination of the open field strength at the Sun from Ulysses magnetometer measurements is also difficult. The radial magnetic field will be strongly affected by stream-stream interactions and CMEs. Nevertheless, a north-south asymmetry in the radial magnetic field was established by combining Wind and Ulysses magnetometer measurements [*Smith et al.*, 2000], indicating stronger fields in the south compared with the north polar coronal hole. Temporal variations, which apparently occurred during the fast latitude scan when Ulysses moved from south to north, probably obscured much of this asymmetry in the Ulysses magnetometer data. *Smith et al.* [2000] reported a ~(6 ± 8)% larger average radial magnetic field strength (r^2B_r = 3.34 nT) from the southern polar coronal hole (averaged between −80° and −20° latitude) than from the northern polar coronal hole (averaged between +80° and +20° latitude) but concluded that this small difference was not significant in view of the large standard error. Averaging $B_{open}(t, \theta)$ over the same latitude intervals, we find a (2 ± 1)% larger average open field strength from the southern coronal hole. Thus the two different determinations of the open field strength agree within errors. Assuming radial expansion, the 3.34 nT average radial field in the southern polar coronal hole measured with the Ulysses magnetometer translates to 1.55 ± 0.10 G at the solar surface, which agrees with the average value of 1.59 ± 0.06 G that we infer.

[49] *Zhang et al.* [2002] reports that ground-based magnetograms show that during the entire 1994–1996 time period the north polar coronal hole covered a larger area of the solar surface than the south coronal hole and that the total magnetic field strength was considerably lower in the northern compared with the southern coronal hole. This is consistent with the data that we present in Figure 5 (top), which shows that the average loop height, and thus $(B/\rho)_{loop}(h)$ (from equation (8) and Figure 4), was also inferred to be ~25% lower in the north than in the south polar coronal hole.

6. Summary and Conclusions

[50] 1. Using SWICS-Ulysses data, we find a strong correlation between the measured solar wind speed, V_{sw}, and the inverse of the electron temperature, T, deduced from measured O^{7+}/O^{6+} density ratios. A good linear fit gives $V_{sw} = 844/T - 88$, with units of km s^{-1} for V_{sw} and 10^6 K for T. An equally good linear fit is found between V_{sw}^2 and $1/T$ of the form $(V_{sw}^2)/2 = 4.42 \times 10^{14}X - 2.31 \times 10^{15}$. Using the data presented here, it is not possible to decide which of these two fits is better.

[51] 2. Other than the theory presented in the companion paper [*Fisk*, 2003], we know of no theory or model that predicts a linear dependence of V_{sw} or V_{sw}^2 on $1/T$. Future solar wind theories must be able to account for the observed inverse linear relationship between V_{sw} and T given above or one closely similar to it.

[52] 3. The loop model proposed by *Fisk* [2003] gives a simple relation (equation (2)) between the speed of the solar wind and electron temperature at its source. This predicted relationship between V_{sw}^2 and $1/T$ is supported by SWICS solar wind observations as shown in Figure 2.

[53] 4. Applying Fisk's formula to SWICS-Ulysses data and using solar observations of loop height distributions, we infer the dependence on loop height of the ratio of the magnetic field strength to mass density near the base of the loops. Using a value of B = 25 G [*Handy and Schrijver*, 2001], we find reasonable values for $\rho_{loop} = 0.85 \times 10^{-14}$ g cm^{-3} (electron density of ~4×10^9 cm^{-3}) near the foot points of the larger loops.

[54] 5. Our simple analysis, which detects sudden large deviations from the ambient relation between V_{sw} and $1/T$, may allow us to identify CMEs lasting a few days or more. Should more detailed studies now in progress confirm our initial results presented here, this technique, which can be implemented in the processing of our data, may provide an easy way for routinely identifying long-duration CMEs.

[55] 6. Applying the same analysis used during the 166-day period to a full solar cycle of SWICS-Ulysses data, we infer the following in the time period between solar maximums (~1992–1997):

[56] • In the quiet Sun, loop heights show a strong dependence on colatitude, reaching heights of ~100,000 km at low latitude. In polar coronal holes the lowest heights (~15,000–30,000 km) were observed, and the loop heights show minimum fluctuation and no apparent latitude dependence. Furthermore, a north-south asymmetry in loop heights is inferred both in coronal holes and in the quiet Sun, with higher loop heights in the Southern Hemisphere compared with the Northern Hemisphere.

[57] • Variations of the inferred average open magnetic field strength in the corona appear to depend on latitude, especially in, but also outside, coronal holes. Strongest open magnetic fields (~1.7 G) are reached at highest latitudes.

Lowest values of the field strength (~1.25 G) are seen shortly after solar minimum.

[58] ● North-south asymmetries are evident for the open magnetic field strength and for loop heights of the polar coronal holes. Similar asymmetries have also been reported in the magnitude of the average heliospheric radial magnetic field and for cosmic rays. Ground-based magnetograph measurements also show similar north-south asymmetries. The north polar coronal hole covers a larger part of the solar surface and has a weaker average magnetic flux and flux density than the south polar coronal hole.

[59] 7. Around solar maximum the dependence of loop heights on colatitude and the latitude dependence of open magnetic fields disappear along with the large polar coronal holes.

[60] Our main conclusion is that the same simple mechanism, expressed by Fisk's solar wind formula, can account for our ionization temperature measurements both in the fast and slow solar wind. From this we infer that the final speed of the solar wind is determined by the temperature of electrons in magnetic loops of the Sun where that wind originates. Very simply, we argue that the fast wind comes from low-temperature loops which are prevalent in coronal holes and that the slow wind originates from higher-temperature loops of the quiet Sun. We suggest that the mechanisms producing both the slow and fast wind are the same, namely, the release of solar wind material from coronal loops by reconnection with open field lines. We would attribute the different plasma properties observed for the fast and slow solar wind to be the result of differences in global coronal conditions, such as loop sizes, configurations, and temperatures, between coronal holes and the quiet Sun. Work now in progress will explore other consequences of the loop theory of the solar wind, including mass fractionation or the first ionization potential effect. These predictions will be tested using solar wind composition data and other relevant observations.

[61] **Acknowledgments.** Discussions with Len Fisk concerning his model of solar wind origin [*Fisk*, 2003] motivated us to initiate this study, and we are indebted to him for many illuminating discussions and numerous suggestions for improving this paper. We thank Jack Gosling for providing us with the Ulysses CME list, Rudolf von Steiger for helpful discussions, and Christine Gloeckler for her assistance with data reduction and programming. We thank the many reviewers of this paper for their most helpful comments and suggestions. This work was supported in part by NASA/JPL contract 955460 and NASA/Caltech grant NAG5-6912.

[62] Shadia Rifai Habbal thanks Marco Velli, Margarita Partenova Ryutova, and John T. Gosling for their assistance in evaluating this paper.

References

Bürgi, A., and J. Geiss, Helium and minor ions in the corona and solar wind: Dynamics and charge states, *Sol. Phys.*, *103*, 347, 1986.

Feldman, U., K. G. Widing, and H. P. Warren, Morphology of the quiet solar upper atmosphere in the $4 \times 10^4 < T_e < 1.4 \times 10^6$ K temperature regime, *Astrophys. J.*, *522*, 1133, 1999.

Fisk, L. A., Acceleration of the solar wind as a result of the reconnection of open magnetic flux with coronal loops, *J. Geophys. Res.*, *108*, doi:10.1029/2002JA009284, in press, 2003.

Geiss, J., et al., The southern high speed stream: Results from SWICS/Ulysses, *Science*, *268*, 1033, 1995.

Gloeckler, G., Observation of injection and pre-acceleration processes in the slow solar wind, *Space Sci. Rev.*, *89*, 91, 1999.

Gloeckler, G., et al., The Solar Wind Ion Composition Spectrometer, *Astron. Astrophys. Suppl. Ser.*, *92*, 267, 1992.

Gosling, J. T., and V. J. Pizzo, Formation and evolution of corotating interaction regions and their three-dimensional structure, *Space Sci. Rev.*, *89*, 21, 1999.

Handy, B. N., and C. J. Schrijver, On the evolution of the solar photosphere and coronal magnetic field, *Astrophys. J.*, *547*, 1100, 2001.

Ko, Y.-K., L. A. Fisk, J. Geiss, G. Gloeckler, and M. Guhathakurta, An empirical study of the electron temperature and heavy ion velocities in the south polar coronal hole, *Sol. Phys.*, *171*, 345, 1997.

Ogilvie, K. W., M. A. Coplan, P. Bochsler, and J. Geiss, Solar wind observations with the ion composition instrument aboard the ISEE-3/ICE spacecraft, *Sol. Phys.*, *124*, 167, 1989.

Parker, E. N., Dynamics of the interplanetary gas and magnetic fields, *Astrophys. J.*, *128*, 664, 1958.

Rosner, R., A brief introduction to coronal "loops," in *Physics of Magnetic Flux Ropes*, *Geophys. Monogr. Ser.*, vol. 58, edited by C. T. Russell, E. R. Priest, and L. C. Lee, p. 189, AGU, Washington, D. C., 1990.

Simpson, J. A., M. Zhang, and S. Bame, A solar polar north-south asymmetry for cosmic ray propagation in the heliosphere: The Ulysses pole-to-pole rapid transit, *Astrophys.*, *465*, L69, 1996.

Smith, E. J., and A. Balogh, Ulysses observations of the radial magnetic field, *Geophys. Res. Lett.*, *22*, 3317, 1995.

Smith, E. J., J. R. Jokipii, J. Kota, R. P. Lepping, and A. Szabo, Evidence of a north-south asymmetry in the heliosphere associated with a southward displacement of the heliospheric current sheet, *Astrophys. J.*, *533*, 1084, 2000.

von Steiger, R., N. A. Schwadron, L. A. Fisk, J. Geiss, G. Gloeckler, S. Hefti, B. Wilken, R. F. Wimmer-Schweingruber, and T. H. Zurbuchen, Composition of quasi-stationary solar wind flows from Ulysses/Solar Wind Ion Composition Spectrometer, *J. Geophys. Res.*, *105*, 27,217, 2000.

Zhang, J., J. Woch, S. K. Solanki, and R. von Steiger, The Sun at solar minimum :North-south asymmetry of the polar coronal holes, *Geophys. Res. Lett.*, *29*(8), 1236, doi:10.1029/2001GLO14471, 2002.

Zurbuchen, T. H., L. A. Fisk, G. Gloeckler, and R. von Steiger, The solar wind composition throughout the solar cycle: A continuum of dynamic states, *Geophys. Res. Lett.*, *29*(9), 1352, doi:10.1029/2001GL013946, 2002.

J. Geiss, International Space Science Institute, Hallerstrasse 6, CH-3012, Bern, Switzerland. (geiss@phim.unibe.ch)

G. Gloeckler, Department of Physics/Space Physics, University of Maryland, College Park, MD 20742-4111, USA. (gg10@umail.umd.edu)

T. H. Zurbuchen, Department of Atmospheric, Oceanic, and Space Sciences, University of Michigan, 2455 Hayward Street, Ann Arbor, MI 48109, USA. (thomasz@umich.edu)